5746–5756 *Nucleic Acids Research, 2013, Vol. 41, No. 11* *Published online 24 April 2013*
doi:10.1093/nar/gkt298

Single molecule analysis of DNA wrapping and looping by a circular 14mer wheel of the bacteriophage 186 CI repressor

Haowei Wang[1], Ian B. Dodd[2], David D. Dunlap[3], Keith E. Shearwin[2,*] and Laura Finzi[1,*]

[1]Department of Physics, Emory University, 400 Dowman Drive, Atlanta, GA 30322, USA, [2]School of Molecular and Biomedical Science, Discipline of Biochemistry, University of Adelaide, Adelaide 5005, Australia and [3]Department of Cell Biology, Emory University, 615 Michael Street, Atlanta, GA 30322, USA

Received January 15, 2013; Revised February 26, 2013; Accepted March 28, 2013

ABSTRACT

The lytic–lysogenic decision in bacteriophage 186 is governed by the 186 CI repressor protein in a unique way. The 186 CI is proposed to form a wheel-like oligomer that can mediate either wrapped or looped nucleoprotein complexes to provide the co-operative and competitive interactions needed for regulation. Although consistent with structural, biochemical and gene expression data, many aspects of this model are based on inference. Here, we use atomic force microscopy (AFM) to reveal the various predicted wrapped and looped species, and new ones, for CI regulation of lytic and lysogenic transcription. Automated AFM analysis showed CI particles of the predicted dimensions on the DNA, with CI multimerization favoured by DNA binding. Measurement of the length of the wrapped DNA segments indicated that CI may move on the DNA, wrapping or releasing DNA on either side of the wheel. Tethered particle motion experiments were consistent with wrapping and looping of DNA by CI in solution, where in contrast to λ repressor, the looped species were exceptionally stable. The CI regulatory system provides an intriguing comparison with that of nucleosomes, which share the ability to wrap and release similar sized segments of DNA.

INTRODUCTION

The CI repressor protein of bacteriophage 186 is proposed to regulate lytic and lysogenic transcription in a unique way—a mechanism involving alternative DNA loops, DNA wrapping and relief of transcriptional interference (1–5). X-ray crystallographic and mutational studies of CI (2,5) support a novel structural model in which seven CI dimers are arranged in a planar ring, or wheel, with the N-terminal DNA recognition domains (NTDs) displayed around the outside (Figure 1A). CI binds with high co-operativity to a large region of DNA encompassing the lytic pR and lysogenic pL promoters (Figure 1B), and binding studies have identified three operators, each spaced two turns of the DNA helix apart, that provide strong pR binding and repression (3,4). However, DNase protection extends some 60 bp to the right of these operators, involving poorly defined recognition sequences over pL that by themselves do not confer CI binding (3). Thus, it is proposed that the pR operators bind to three adjacent CI dimers on the wheel, and that the resulting proximity of the pL DNA allows weaker interactions to cause this DNA to 'wrap' onto three of the remaining CI dimers on the wheel (Figure 1), causing co-ordinate repression of pR and pL (2,3).

CI also binds to two distal operators, FL and FR, located ~300 bp from the pR–pL region (4). These sites have two major effects on regulation by CI *in vivo*: they assist CI repression of pR, and they allow CI to activate pL (3). These effects are proposed to involve DNA loops in which the FL or FR operators bind to a CI wheel bound at pR–pL (1,2). The presence of seven CI dimers on the wheel means that it should be able to bind simultaneously to the three pR operators and either FL or FR (2). Co-operative binding to FL or FR should, therefore, strengthen CI occupation of pR. However, structural considerations suggest that the wheel bound to the pR operators is not large enough to accommodate FL or FR and the wrapped pL sequences. Thus, it is proposed that FL and FR binding to the pR–pL wheel displaces the pL sequences from the wheel, providing RNA polymerase

*To whom correspondence should be addressed. Tel: +1 404 727 4930; Fax: +1 404 727 0873; Email: lfinzi@emory.edu
Correspondence may also be addressed to Keith E. Shearwin. Tel: +61 8 8313 5361; Fax: +61 8 8313 4362; Email: keith.shearwin@adelaide.edu.au
Present address:
Haowei Wang, Department of Physics, University of Toronto, ON L5L 1C6, Canada.

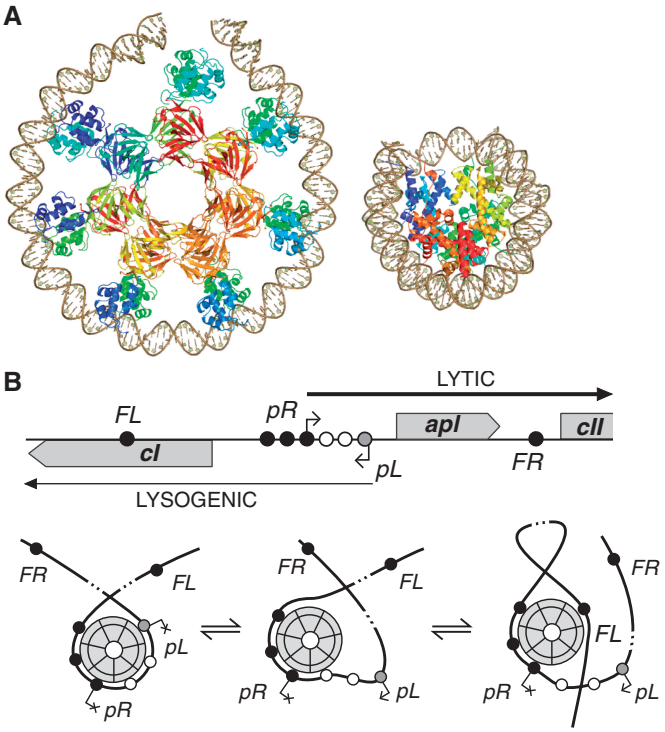

Figure 1. Models of phage 186 CI structure and action. (**A**) (Left) Composite structural model of the CI 'wheel' based on X-ray structures of the central 14mer C-terminal domain (PDB:2FKD), a full-length CI mutant (PDB: 2FJR), which does not associate beyond dimers, and a 145-bp segment of DNA. The CI–DNA complex has a predicted diameter of 17.5 nm and height of 6 nm. (Right) Core '601' nucleosome structure containing 145 bp of DNA (PDB: 3LZI), at the same scale. (**B**) Diagram (not to scale) showing the CI-binding sites at the 186 switch region (unfilled circles are poorly defined weak sites), and the proposed control of pR and pL by wrapping of DNA around the wheel, with the distal FL (shown) or FR sites able to de-repress pL by competing for wheel binding.

access to pL (2) (Figure 1B). The convergent arrangement of pR and pL causes the strong pR to suppress the weaker pL by transcriptional interference (6) and this suppression can be relieved by CI repression of pR (3,7). It is proposed that FL or FR is needed for the indirect activation of pL by CI because by displacing pL from the wheel they allow CI to repress pR without also repressing pL.

The *in vivo* effects of a range of CI concentrations on pR and pL activity in the presence or absence of FL, FR and pR were reproduced in a mixed statistical–mechanical/kinetic model that invoked a variety of different CI–RNAP–DNA species, involving up to three CI wheels binding in different ways to the FL, pRpL and FR sites (1).

Although DNA wrapping and looping to a 14mer CI wheel provides a plausible model for CI action, many aspects of the model are based on inference and have not been directly confirmed. The 14mer wheel model for CI is an inferred composite structure assembled from a 14mer structure of the CI C-terminal domain (CTD) and a structure of a full-length dimeric CI mutant (2). Although these structures are consistent with the locations of mutations that disrupt the monomer–monomer and dimer–dimer interfaces, the full wheel structure has not been directly observed. In the dimeric structure, the N-terminal domains pack in a way that is unlikely to allow DNA binding. In the full wheel structural model, these domains have been moved relative to each other and relative to the CTDs to position their helix-turn-helix (HTH) domains so that they could contact the major grooves of the three adjacent pR operators with a two DNA turn phasing. This phasing predicts that up to ~147 bp (14 turns) of DNA, similar to that wrapped around a histone octamer, could be wrapped around the full wheel (Figure 1). However, no CI–DNA structures or DNA wrapping data are available to validate this proposed model.

The regulatory model involves CI wheels binding at FL, pR-pL and FR, but it is not known whether the full wheel is the major binding species or whether smaller multimers of CI are significant binding species. The idea that the pL DNA adjacent to the pR operators can wrap onto the wheel, although consistent with binding and gene expression data, has not been confirmed. In addition, DNA looping between the three major binding sites is inferred from co-operativity observed in gene expression studies, but looping between sites has not been directly demonstrated.

Here, we describe a series of single-molecule experiments that provide direct evidence for a number of these features of the CI–DNA binding model. Atomic force microscopy (AFM) imaging of CI–DNA complexes revealed each of the predicted wrapped and looped species. Automated analysis of AFM images showed CI commonly takes a form on the DNA with dimensions consistent with the 14mer wheel on DNA, and that the wheel may be able to 'roll' along the DNA. Tethered particle motion (TPM) experiments demonstrated DNA shortening events consistent with both DNA wrapping and DNA looping and showed that these CI–DNA loops are long-lived in solution.

MATERIALS AND METHODS

Protein preparation

CI–His_6 and CI(HTH^-)His_6 were prepared as described previously (5) and stored at −80°C in TEG150 buffer [50 mM Tris–HCl, 150 mM NaCl, 0.1 mM ethylenediaminetetraacetic acid and 10% glycerol (pH 7.4)].

AFM sample preparation

The 1584-bp-long DNA fragments were produced by cutting the pBS-HSL series of plasmids (Supplementary Data) containing wild-type or mutant 186 operators (FL, pR-pL and FR) with NgoMIV and XmaI (New England BioLabs). The required digestion product was gel extracted and purified (QIAGEN gel purification kit).

For higher resolution AFM studies using smaller DNA fragments, the following primer pairs were used to amplify DNA fragments from the pBS-HSL series of vectors containing either the FL or the pR operators:

5′-TTACCGGAGAAGGAGAAGCA-3′ and 5′-biotin-ATTAATGCAGCTGGCACGAC-3′ generated a 524-bp-long DNA containing only the FL operator.

The 5′-biotin-CTTTCTTGCAGCCTTTACGG-3′ and 5′-TTTACAAATGCTTCTCCTTCTCC-3′ generated a 528-bp-long DNA containing only the pR and pL operators, with a biotin tag on the pR proximal side.

CI samples were diluted to the desired final concentration (5, 50 and 100 nM) in the presence of 1 nM DNA in a buffer containing 50 mM HEPES, 150 mM NaCl and 0.1 mM ethylenediaminetetraacetic acid (pH 7.0). All steps were conducted at T_{room}. The mixture was incubated for 20 min. The biotin-labelled DNA fragment was incubated in a mixture containing also 1 μg/ml of streptavidin. Shortly before deposition, a 10-μl drop of 0.01 μg/ml of poly-L-ornithine (1 kDa MW, Sigma-Aldrich, St. Louis, MO, USA) was incubated on freshly cleaved mica for 1 min. The poly-L-ornithine-coated mica was then washed with 0.4 ml of high-performance liquid chromatography grade water and dried with compressed air. Then, 10 μl of the solution containing DNA and protein was deposited on the poly-L-ornithine-coated mica and incubated for 1 min. The droplet was rinsed with 0.4 ml of high-performance liquid chromatography grade water and dried gently with compressed air. The sample was left to dry overnight on the bench or in a dessiccator for a few hours before imaging.

Images were acquired with a NanoScope IIIa MultiMode AFM microscope (Digital Instrument, Santa Barbara, CA, USA) operated in tapping mode using uncoated, etched silicon tips (MirkoMasch, San Jose, CA, USA). The oscillation amplitude was 50–60 mV with a resonance frequency of 75 kHz. Areas of $1 \times 1\,\mu m^2$ were scanned at a rate of 1.2 Hz and with a resolution of 512×512 pixels.

After filtering images to remove scan line offsets and bowing, DNA molecules were interactively traced with NeuronJ (8), a plug-in for ImageJ (9). We also developed a new image analysis algorithm, written in MATLAB (Supplementary Data) for unbiased high-throughput analysis.

Tracing of unbound DNA ($n = 103$) gave a length to base pair conversion factor of 0.32 nm/bp of DNA with a measurement error of 2.2% (Supplementary Figure S6).

TPM experiments

The 1898-bp-long wild-type or mutated DNA segments were produced by polymerase chain reaction as described in Supplementary Data.

The TPM microchamber and experiment were prepared and run as previously described (10–12). In brief, the glass surface of a microscope flow chamber was coated with biotin–labeled bovine serum albumin and incubated with streptavidin. DNA tethers were labelled with anti-digoxigenin–coated beads with a diameter of 0.48 μm (Indicia Diagnostics, Oullins, France) and observed through a differential interference contrast microscope equipped with a ×100 oil-immersion objective (N.A. = 1.25). For each DNA tether, 10 min of data was recorded before adding 186 CI protein. In all, 50 nM of CI protein and 1 nM of competitor DNA (short fragments that contain specific sites but are unable to interact with the surface or the beads) were added, and another 20 min of data was recorded. Interaction of the 186 CI protein with DNA was monitored as a reduction in the amplitude of the Brownian motion of the bead in the x–y plane, as previously described (10,13–15). The mean square deviation ($<\rho_{\perp}>$) was converted into base pairs of DNA shortening using a calibration curve (Supplementary Figure S8).

RESULTS

AFM reveals the predicted CI–DNA complexes

Direct identification of the individual CI species in our gene regulation model requires single-molecule techniques. AFM was used to image CI bound to a 1584-bp DNA fragment encompassing the FL, pRpL and FR binding sites (Figure 2A and B). For the purpose of comparison, Figure 2C and D shows an AFM image of DNA wrapped around histones and a DNA loop mediated by λ repressor. By tracing the distance from the DNA ends to the CI particles in the AFM images, the vast majority of CI binding was seen to be distributed in three broad peaks centred at the three sites, with occupation frequency ranking pRpL > FL > FR (Figure 2A), consistent with previous affinity estimates (4).

Figure 2B shows examples of the different CI–DNA species observed at 50 nM CI and their relative frequencies across 315 unambiguously interpretable DNA fragments. We observed all but one of the 14 different CI-bound species predicted by the gene regulation model. The lack of observation of a species with a CI particle bound only to FR is explained by the weakness of binding to this site relative to FL and pRpL. Most of the DNA-bound particles exhibited DNA wrapping to various extents around the perimeter of the particles, consistent with the structural model (Figure 1A). Extensive DNA wrapping was expected at pRpL, where there are three well-defined binding sites, but substantial wrapping was also seen at FL and FR.

Importantly, all six predicted CI–DNA looped species were observed (Figure 2B). In all cases, the loops involved two CI-binding sites (any pairwise combination of FL, pR and FR) binding to a single CI particle. First, these direct observations of DNA looping confirm the conclusions from the regulatory studies that CI binding to these separated sites is co-operative. The ability of a CI particle at pR to simultaneously bind to FL or FR species increases the fractional occupation of pR, seen as increased repression of pR in the presence of the distal sites (3). Second, the lack of images in which all three DNA sites are bound to the same CI particle (which were specifically searched for) confirms a critical prediction that only two non-contiguous DNA segments can bind to the same CI wheel (1,2). Such competition for space on the CI wheel is proposed to result in displacement of pL from a pRpL-bound wheel on co-binding of FL or FR, allowing RNAP access to pL. The relative frequency of looped complexes in the AFM images was low compared with expectations from modelling *in vivo* regulation by CI. For example, at a CI concentration for

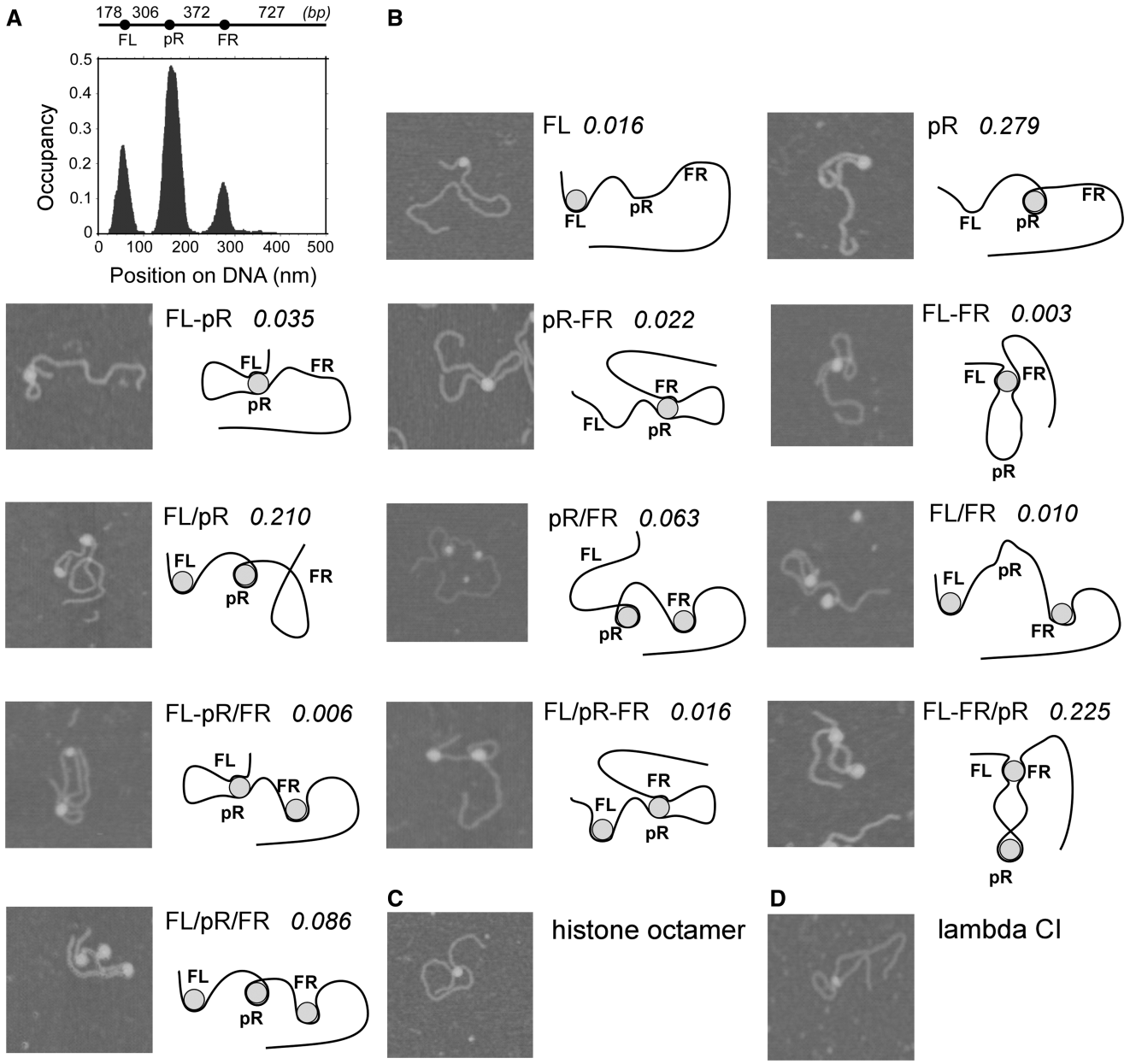

Figure 2. AFM analysis of CI–DNA complexes. (**A**) Histogram of CI occupancy along the 1584-bp linear DNA fragment in AFM images ($n = 315$). The DNA diagram in base pairs is aligned above the histogram to highlight the correspondence between the measured distances in nm with the expected distances in bp. For the histogram, the position of CI particles on the DNA was determined by tracing from the centre of the DNA bound to or wrapped around the particle(s) to each end of the molecule. For each DNA, the orientation most consistent with the locations of FL, pR and FR was chosen and the distances from the left end of the DNA plotted on the histogram. (**B**) Selected AFM images of CI particles bound to DNA, showing species predicted by the wheel binding model. A schematic drawing of the type of species and the fraction of each species in 315 interpretable complexes are shown (0.025 had no CI, no DNA molecules had FR bound only). (**C**) AFM image of a histone octamer bound to a 601 nucleosome positioning sequence in the 1414-bp SapI–XmnI fragment of pGEM3Z-601. (**D**) AFM image of λ repressor bound to λ OR and OL operators.

which the three-wheel species makes up 9% of the total, as in Figure 2, the two single CI particle species where pR loops to FL or FR would be expected to comprise ~25% of the total (1), substantially more than the 6% seen by AFM. These differences may be due to differences between *in vivo* conditions and the AFM experiments, such as different salt conditions, the presence of nucleoid proteins and RNAP *in vivo*, the effects of *in vivo* DNA supercoiling and the constraints of 2D deposition in AFM.

Two species that were observed in the AFM images, but which were omitted from the published regulatory model, are those with FL and FR bound to a single wheel, either with or without an additional wheel at pR (two-wheel FL–FR/pR species and one-wheel FL–FR species, Figure 2). The first species is common, comprising 22% of those seen

with wild-type DNA. It seems possible that DNA bending caused by the wheel at pR could bring FL and FR together, favouring their interaction and making it more likely that they bind to the same CI wheel. However, the number of two-wheel FL–FR/pR complexes seen in AFM images is not more than expected for independent CI binding to FL–FR and to pR ($P = 0.47$, χ^2 test).

CI particle dimensions are consistent with the structural model

Next, we asked whether the particle sizes observed by AFM were consistent with the composite structural model of the wheel shown in Figure 1. AFM measurements provide information about the X, Y and Z dimensions of the particle adsorbed to the surface, enabling measurement of particle volume. An automated analysis procedure written in MATLAB (Supplementary Data) was designed to provide an unbiased assessment of the distribution of CI particle diameter and volume, across a large number of particles in the AFM images. This procedure relies on analysis of measurements at a defined height (31% of the particle height) above the mica surface, such that for CI–DNA complexes, the DNA itself is not expected to contribute significantly to the particle dimensions. This analysis was performed on CI in the absence of DNA, CI in the presence of control DNA containing no specific CI sites and CI in the presence of wild-type (1584 bp) 186 DNA containing all three operator regions (Supplementary Table S1–S4). As a further control, we also used a DNA-binding defective version of CI, designated CI HTH$^-$, which carries amino acid changes within its HTH DNA recognition motif, but multimerizes normally (5).

First, we examined particle volume (Supplementary Figure S2 and Supplementary Table S2). Because of the effects of tip broadening, to relate measured volumes to molecular weight, the measured particle volumes need to be compared with a calibration curve, previously obtained using proteins of known size (16) and supplemented in this study with an additional measurement of the volume of a histone octamer (Supplementary Figure S1). The measured volume of the 186 CI particles in the presence of specific 186 DNA ($632 \pm 152\,nm^3$; $n = 975$) is consistent with the molecular weight of a 6His-tagged CI 14mer ($22\,590 \times 14 = 316$ kDa) (Supplementary Figure S1). Our calibration curve is remarkably similar to one recently published using a fiducial marker for precise volume calibration (17).

Second, we examined the diameter distribution of CI particles in the presence and absence of DNA (Supplementary Figure S2 and Supplementary Table S3). With CI HTH$^-$, only one major peak was observed at ~14 nm (13.2 ± 1.9 nm for no DNA, 14.5 ± 1.4 nm for lambda DNA and 13.9 ± 1.0 nm for 186 DNA). This mean diameter is smaller than that predicted for intact 14mer wheels, consistent with incomplete wheel formation in the absence of DNA and at this low concentration of CI. In the absence of DNA, the wild-type protein had a diameter similar to that of CI HTH$^-$ (15.0 ± 1.4 nm). However, the average diameter of particles increased when 186 CI was incubated with non-specific DNA (17.2 ± 1.4 nm), and even more in the presence of 186 wild-type DNA, to 19.5 ± 1.7 nm ($n = 975$).

To further test how the particle dimensions determined by AFM should relate to those predicted from the composite structure, a mathematical simulation was developed, taking into account the relative dimensions of the predicted CI wheel and AFM tip (Supplementary Figures S3 and S4; Supplementary Data). These simulations also supported the wheel model, indicating that a half ellipsoid with the dimensions of the proposed CI 14mer would be detected under these AFM conditions as a particle ~748 nm^3 in volume and 18.7 nm in diameter.

We also examined CI multimerization at higher concentrations using size-exclusion chromatography combined with multi-angle laser light scattering (SEC–MALLS). Wild-type CI (calculated monomeric Mw 22 590) at a loading concentration of 146 μM gave a weighted average molecular weight across the peak of $280\,000 \pm 8000$, corresponding to 12.4 monomers (Supplementary Figure S5). Similarly, the mutant CI-HTH$^-$ protein gave a Mw of $274\,000 \pm 5000$ and a calculated stoichiometry of 12.1 monomers. Previous analytical ultracentrifugation studies showed that CI is predominantly dimeric at nanomolar concentrations and forms higher order multimers at micromolar concentrations (5,18). The equilibrium between CI dimers and higher order multimers is thus pushed towards multimers at the high-CI concentrations used in the SEC–MALLS experiments.

Taken together, these biophysical measurements are consistent with the CI–DNA structure shown in Figure 1, a structure whose production is favoured by the presence of DNA containing its specific operator sequences.

DNA wraps onto CI wheels

In AFM images of CI–DNA, the DNA was almost always wrapped around the outside of the complex in what seemed to be a single coil (Figure 2), consistent with the structural model for DNA binding (Figure 1A).

The lengths and positions of the wrapped DNA segments at FL and at pR were quantitated by tracing the length of DNA on either side of the CI wheel in AFM images using short (~500 bp) DNA fragments labelled at one end with biotin–streptavidin (Figure 3A–C). Both the length and the position of the CI-bound DNA segments were highly variable on both templates. The observed variability was much greater than that expected from the error in length measurements (Supplementary Figure S6), suggesting that CI is able to move on the DNA by wrapping or releasing DNA on either side of the wheel. There was substantial variation in the proportion of the wheel's circumference contacted by DNA, with this degree of wrapping generally greater at pR than at FL. At FL, the length of the wheel-associated region of DNA ranged from 5 to 160 bp (median 101 bp; Figure 3D). At pR, the distribution of wrapping lengths ranged from 54 to 310 bp (centred at 184 bp; Figure 3E). Thus, at both sites, the amount of DNA wrapped was usually more than could be explained solely by occupation

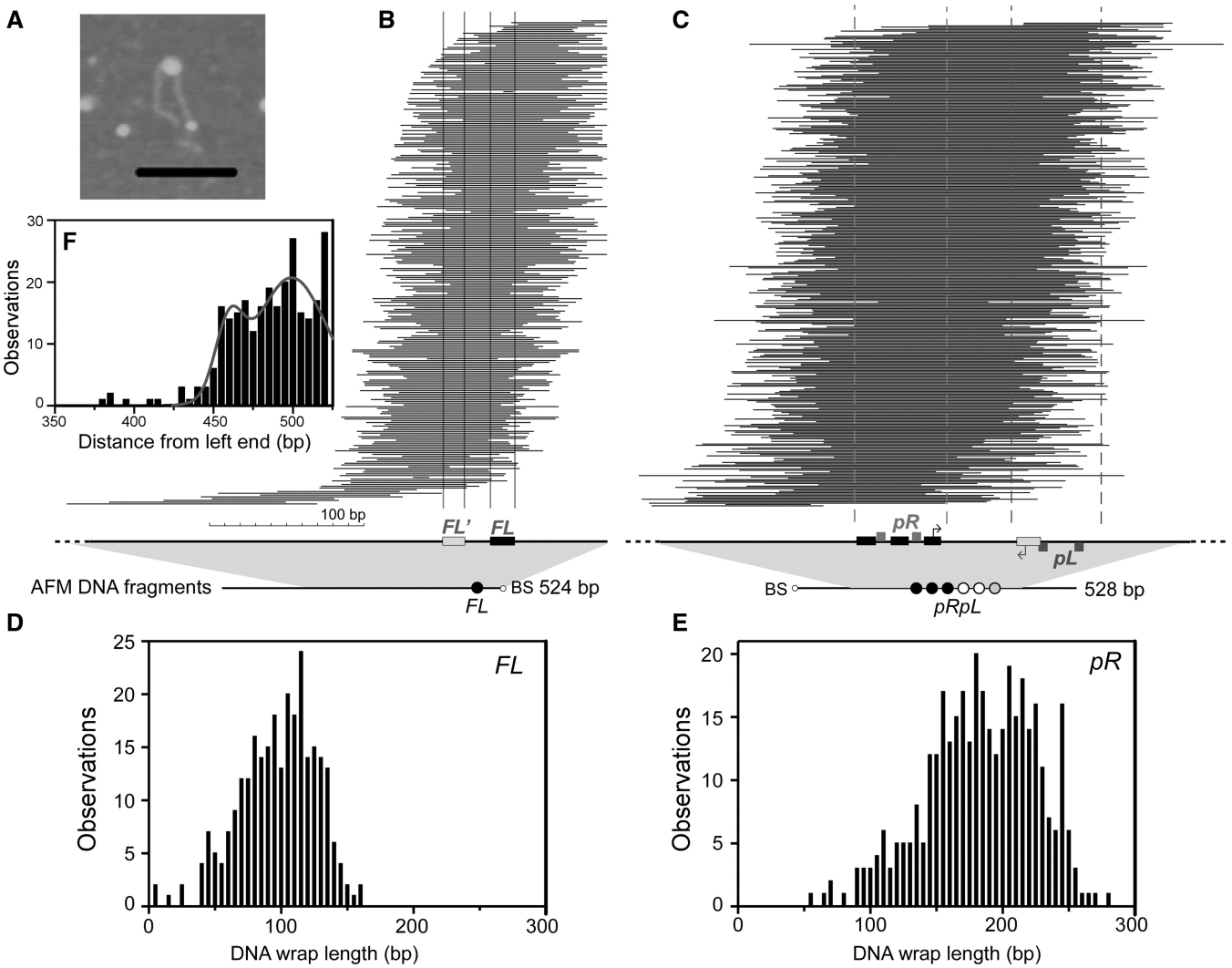

Figure 3. Heterogeneous CI binding at FL and pRpL. (**A**) AFM image showing a 186 CI–DNA complex with a streptavidin fiducial marker at one end of the DNA. Scale bar = 100 nm. (**B** and **C**) Horizontal lines show the extent of individual CI-bound portions of biotin–streptavidin (BS) end-labelled DNA fragments containing FL (A; $n = 272$) or pR (B; $n = 368$) in AFM experiments. Line lengths are drawn at the same scale for FL and pR. The location of the FL operator and the putative FL′ operator is marked by vertical lines. The −10 and −35 sequences for pR and pL and the CI recognition sequences at pR and pL are shown by boxes. The dashed lines indicate the +10 to −50 promoter regions where CI binding is expected to repress pR or pL. (**D** and **E**) Frequencies of the lengths (bp) of DNA wrapped onto CI particles at FL and pR. (**F**) Frequencies of distances (bp) between CI and the labelled end of the FL DNA fragment, showing a bimodal distribution.

of the defined operator sequences [three operators spanning 56 bp at pR, single 17-bp operators at FL (4)].

At FL, the mean centre of binding was located some 18 bp to the left of the centre of the FL operator, indicating an unequal preference for sequences on either side of the operator. This is consistent with DNase footprinting, which showed CI effects extending 64 bp to the left of the FL operator but only 9 bp to the right (4). Interestingly, the distribution of the edges of the DNA-wheel boundary showed some indications of bimodality (Figure 3F). Fitting the histogram of the position of the right-hand edge of the wheel-DNA boundary to two normal distributions gave one peak centred over the right edge of the FL operator and a second peak centred ~30 bp further rightward. If the histogram of the left-hand side of the wheel-DNA boundary is similarly fitted, the two peaks are ~30 bp further to the left edge of FL operator. This suggests the possible existence of a second FL operator, separated by approximately three turns of the DNA helix. Indeed, a DNA sequence centred 30.5 bp to the left of the FL operator shows similarity to the A' class of CI-binding sequence [(4); Supplementary Data] and may be a cryptic operator for CI (FL').

A much larger wrapped region was seen at pR, and as at FL, the left and right boundaries of the wheel were highly variable. Most wheels were in contact with all three, or at least two of the pR operators (87.9% and 96.5%, respectively). In very few cases (2.1%) was the wheel located such that RNAP would be able to bind to pR. Wrapping beyond the three pR operators was biased slightly to the right side, towards pL, consistent with the DNase footprinting data where CI effects extended 70 bp

to the right of the pR operators and just 30 bp to the left [(4); Figure 3C]. Presumably, this reflects sequence features in the DNA surrounding the pR site that aid CI interactions. In most cases, pL is at least partly wrapped onto the wheel but in 30/368 complexes (~9%) the wrapping leaves pL accessible to RNAP (Figure 3C). This is consistent with gene expression data with an isolated pRpL DNA region in which CI represses pR more strongly than pL (1,4).

Although the variable wrapping of DNA beyond the defined operator sequences onto the CI wheel fits the structural model, the length of the entire wrapped region is often substantially longer than the maximal 14 DNA turns (~147 bp) expected with two turns per CI dimer. At pR, 79.4% of occupied segments are longer than 147 bp and average close to 181 bp. In no case was a pair of side-by-side wheels seen at FL or pR. AFM measurements of the heights of the CI–DNA complexes also excluded the possibility of vertical stacks of two or more wheels around which extra coils of DNA could be wrapped (Supplementary Figure S3). Therefore, it seems like CI dimers in a 14mer wheel may not always bind consecutive DNA segments, but perhaps it can also bind segments separated by more than two turns of the helix.

TPM measurements (10,12,13) with 1898 bp DNA fragments, in which FL or pR was the only intact CI-binding site, were used to further examine DNA wrapping at these sites. In these measurements, the amplitude of the Brownian motion of beads tethered by single DNA molecules to the surface of a microscope flowchamber is monitored in real-time. Any change in this amplitude reflects changes in the end-to-end distance of the tether, which, in turn, is indicative of protein-mediated conformational changes. Here, the parameter measured in a TPM experiment is the mean excursion of the bead in the x–y plane, $<\rho_{\perp}>$, averaged during 4 s window (14) (Supplementary Figure S7). These values can then be converted to changes in DNA length by means of a calibration plot obtained under identical conditions with a series of DNA tethers of known length (Supplementary Figure S8). Addition of CI into the microchamber caused an immediate and stable decrease of the TPM signals for both the FL^- pR FR^- DNA (Figure 4A) and for the FL ΔpR FR^- DNA (Figure 4B). Traces were recorded for up to 20 min but did not show reversible transitions between the long and short conformations. From the calibration plot, the observed initial changes in TPM signal are equivalent to shortenings of the DNA tether by ~200 bp. Such shortenings are consistent with the wrapping of long lengths of DNA around CI at these sites. Importantly, these TPM measurements confirm that the characteristics of 186 CI binding at pR and FL detected by AFM are maintained. The histograms confirmed wrapping at both pR and FL and showed that there is more variability (the histogram is wider) in the amount of DNA that may be wrapped around a wheel bound at FL, than at pR.

DNA looping and TPM

The 186 repressor-mediated looping in solution was investigated by TPM with DNA tethers containing two or all three binding regions at their normal spacing (Figure 4C–E). Because wrapping of DNA at single sites produces substantial shortenings (see earlier in the text), it was difficult to unambiguously identify shortenings because of DNA looping, particularly because looping reduces the degree of wrapping and releases some DNA from the wheel. In addition, the histograms of TPM signals may be broadened by non-specific binding interactions. However, in some cases, the TPM traces showed transitions between different shortenings that are likely to be indicative of gain or loss of DNA loops, as shortening because of wrapping seems to be stable (see earlier in the text).

FL^+ ΔpR FR^+ DNA tethers (Figure 4C), which displayed just one peak after addition of repressor, could be separated into two groups. One group of DNA tethers showed an average 8.8 ± 2.3 nm decrease of $<\rho_{\perp}>$, equivalent to 160 bp. This is a smaller shortening than the 11.3 nm seen for FL alone (Figure 4B) and perhaps reflects partial wrapping of a single wheel bound at FR or FL. Another group of tethers showed an average $\Delta<\rho_{\perp}>$ of 26.5 ± 4.3 nm, corresponding to ~410 bp shortening of the DNA. This may be consistent with formation of two fully wrapped wheels at FL and FR. It seems unlikely that this shortening is due to loop formation between FL and FR, as the distance between these sites is 678 bp (Figure 2A). However, looping between FL and FR may not be completely excluded given the tail of the $<\rho_{\perp}>$ distribution. There were no FL^+ ΔpR FR^+ DNA tethers that displayed transitions.

TPM measurements performed on DNA tethers containing only FL and pR (Figure 4D) showed an average 15.2 ± 6.5 nm decrease in $<\rho_{\perp}>$, corresponding to a ~260 bp shortening of the DNA tether. These shortenings may simply be the sum of wrapping and bending at pRpL and at FL. However, the broad distribution of DNA shortening may also be consistent with some changes involving a loop between FL and pR. This loop would consume some 300 bp of DNA (giving an expected $<\rho_{\perp}>$ change of 18 nm) if the two binding sites came in direct contact, but if the sites are bound to opposite sides of the wheel, this could reduce the change in $<\rho_{\perp}>$. Looping seems to occur in three of the 43 FL^+.pRpL.FR^- DNA tethers that displayed transitions and gives a histogram with two peaks, one at 18.9 (± 4) nm and the other at 0 (± 4.5) nm. These probably correspond to the state in which DNA is looped between FL and pR and the unlooped DNA.

After addition of repressor to wild-type 186 DNA, most ($n = 26$ of 31) of the tethers adopted either one of two conformations, characterized by an average decrease in $<\rho_{\perp}>$ of 14.0 ± 6.5 nm (most probable) or of 40.6 (± 3.6) nm, corresponding to a shortening of the DNA tether of ~240 and 580 bp, respectively (Figure 4E). Within experimental error, the 240 bp shortening is equivalent to the one associated with a full wrapping event at pR, but it is indistinguishable from a looping event between pR and either FL or FR. The 580 bp shortening may be interpreted as either wrapping of the DNA around three wheels, bound one to each operator (FL, pR and FR), or to the formation of a loop between

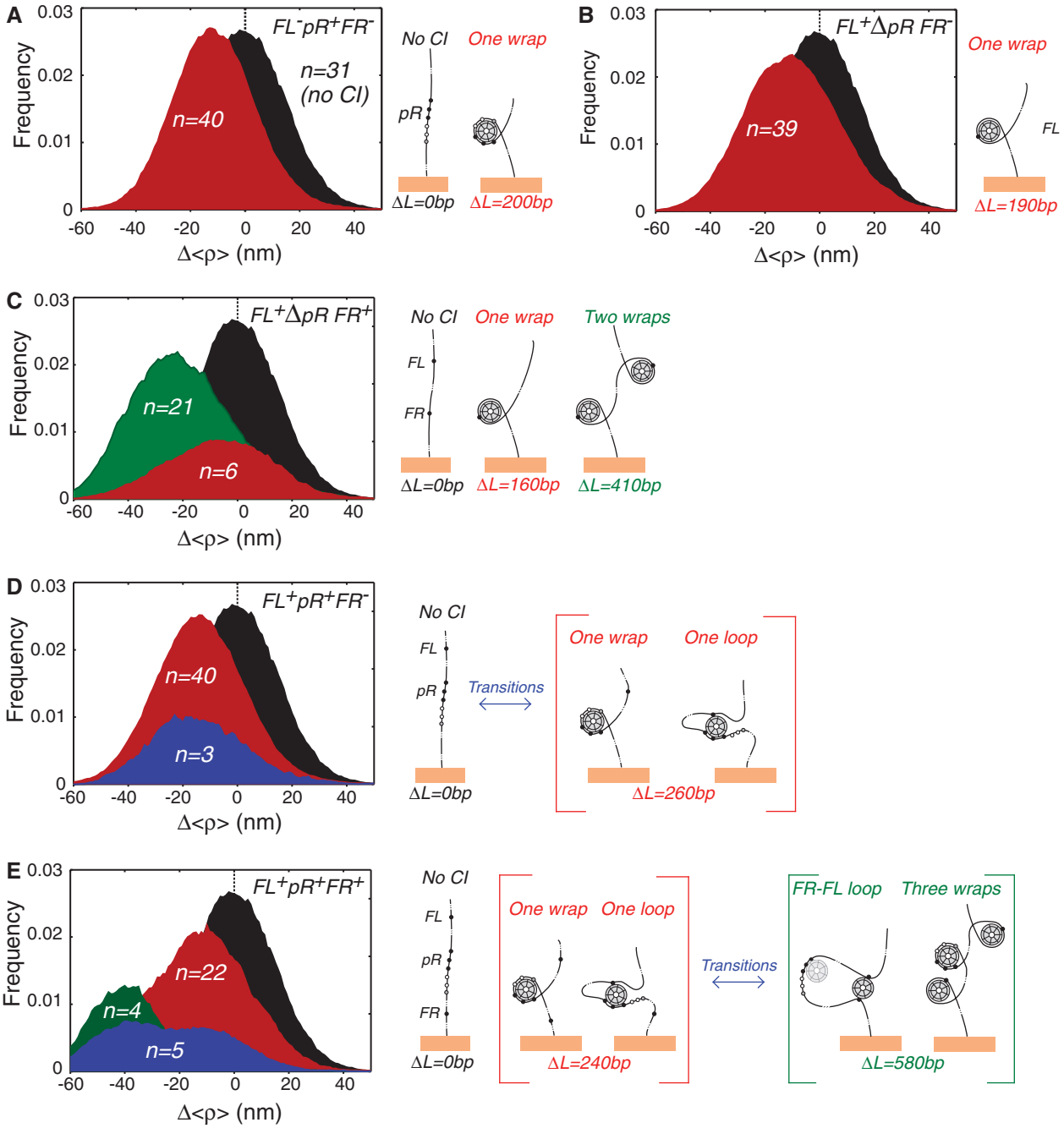

Figure 4. Frequency distribution histograms of TPM data for 1898-bp-long DNA tethers containing combinations of intact 186 CI-binding sites in the presence or absence of 50 nM 186 repressor. In each case, between 25 and 45 tethers were analysed. The TPM data are reported on the *x*-axis as the difference between the average $<\rho_\perp>$ value for the no-CI control (black) and the average $<\rho_\perp>$ value in the presence of CI, $\Delta<\rho_\perp>$. (**A**) When only pR is present, $<\rho_\perp>$ decreases by 11.7 ± 3.9 nm, equivalent to a 200 bp, which is consistent with a 186 wheel fully wrapped by DNA. (**B**) When only FL is present, $<\rho_\perp>$ decreases by 11.4 ± 4.8 nm, equivalent to a 190 bp shortening, which is also consistent with a 186 wheel fully wrapped by DNA. (**C**) When the binding sites at pR are deleted, the tether shortening observed cluster into two groups: one consistent with one wrapping event (8.8 ± 2.3 nm; 160 bp) and another that could represent wrapping events at both FL and FR (26.5 ± 4.3 nm; 410 bp). (**D**) In the absence of FR, many DNA tethers are stably shortened by 15.2 ± 4.5 nm, corresponding to ~260 bp, which is consistent with a loop between FL and pR (including the size of the 186 wheel). Some of the tethers (blue peak) display brief transitions back to the unlooped or partially wrapped state (shoulder at 0 nm). The broad distribution of measured reductions in $\Delta<\rho_\perp>$ may result from tethers where the DNA wraps around the 186 repressor either at pR or at FL (supported by AFM, Figure 2). (**E**) Wild-type DNA in the presence of protein shows a shortening (red peak) of 14.0 ± 6.5 nm (240 bp), which may correspond to a full wrap at pR, or a loop between pR and either FL or FR. Some tethers (green) were shortened to 40.6 ± 3.6 nm (580 bp). This peak is consistent with a conformational state where there is a wheel bound at each of the operators (3 × ~190 bp) or a state where a wheel is mediating a loop between FR and FL (Figure 2). Most often these states are stable for the duration of the measurements, but some transitions were observed between the wrapped and looped configurations (bimodal histogram, blue). Notice, however, that the distribution is broad and probably includes many of the species observed by AFM imaging.

FL and FR, as the distance between the centres of these two operators is 678 bp. In this looped state, a second wheel may be bound at pR, but it would not cause a detectable TPM signal. Of the 31 molecules that were analysed, only five displayed just one or two transitions between the two states in 20 min of observation, but never back to the free DNA state. Their frequency histogram was, therefore, bimodal.

DISCUSSION

Support for the model

The biophysical experiments presented here confirm a number of aspects of the structural-regulatory model for 186 CI.

First, AFM images confirmed that the DNA binds around the outside of the CI particles. As expected, large regions of DNA were able to wrap around the wheel. Importantly, when a CI wheel was bound at pR, the adjacent pL DNA was in most cases, but not always, also wrapped onto the wheel. TPM data on DNA tethers containing only a single operator were also consistent with wrapping of the DNA around the wheel.

Second, AFM showed that CI at relatively low concentrations forms particles with dimensions consistent with CI 14mers. These large wheel-like particles were the primary DNA-bound species. Few 14mer particles were observed in AFM images in the absence of DNA. Instead, a range of smaller particles was seen. Previous ultracentrifugation studies of CI oligomerization in the absence of DNA showed that higher order multimers, such as hexamers or octamers, are rare at the low CI concentrations found *in vivo* (5,18). SEC–MALLS confirmed the existence of 14mers at higher concentrations. The AFM results show that this discrepancy can be resolved by DNA favouring CI multimerization.

Third, AFM images confirmed that any pair of the three CI-binding sites, pR, FL and FR, could simultaneously bind to the same CI wheel to form the DNA loops predicted by the model. TPM showed evidence of DNA shortenings consistent with the size of a loop between pairs of distant CI-binding sites.

Extending the model

The experiments also indicate additional features of CI DNA binding that extend the model.

AFM measurements revealed large variation in the positioning and the amount of DNA occupied by CI wheels at FL, pRpL and FR. This variation suggests that CI binding could be highly dynamic, maintaining the interactions with the strong recognition sites but with the less strongly interacting DNA on either side constantly wrapping and unwrapping on and off the remaining dimers on the wheel. Such a large DNA contact surface also suggests that non-specific binding could be strong, consistent with the binding to other sites seen in the AFM images. Interestingly, it is plausible that CI bound non-specifically could move along the DNA in a unique way, rolling by unwrapping DNA on one side while wrapping DNA on the other. These suggestions were supported by the width of the histograms of the TPM data.

The AFM measurements also revealed a potential additional CI-binding site at FL (FL′) that warrants further investigation. Although the presence of these sites does not require a change to the basic model, it is possible that we have underestimated the importance of FL because there may be some residual CI-binding activity in the FL^- mutants used in previous experiments (3). Notably, this notion was supported by the fact that the TPM data for the $FL^+\Delta pR\ FR^+$ DNA were more widely distributed than the $FL^-pR^+FR^+$ DNA.

The basic regulatory model only requires FL and FR to be able (individually) to form loops to a wheel at pRpL, but AFM images also revealed complexes with FL and FR binding together to their own wheel. The species with one wheel bridging FL and FR and another wheel at pRpL comprised 20% of the wild-type DNA particles. Introduction of this species into the statistical–mechanical model would allow for an effect that is seen in the gene regulation data of Dodd and Egan (3), where repression of pL at higher CI concentrations is stronger if both FL and FR are present. This feature can be reproduced in the modelling if the bringing together of FL and FR by one CI wheel increases the wrapping of pL onto the other wheel at pRpL. Unfortunately, it is not possible to resolve the pL occupancy in the AFM images with full-length DNA.

An inconsistency with the model?

One result seems to be inconsistent with the structural model. Measurements of the length of DNA extending either side of a CI wheel bound at pRpL indicated that the length of DNA in close contact with the wheel was frequently larger than the 12–14 turns of DNA expected if adjacent CI dimers contact sites two DNA turns apart (Figure 1). Accounting for the combined error involved in two tracing measurements, we estimate from these measurements that the wheel is able to occupy ~180 bp of DNA.

One possibility is that there may be a larger DNA spacing between CI dimers. Binding of adjacent CI dimers to sites three turns apart would be consistent with occupation of ~180 bp of DNA by a 14mer. Accommodating this spacing between every CI dimer without significant DNA distortion would require moving the NTDs some 3.9 nm further away from the wheel centre. CI does bind with high affinity to a pair of A-type recognition sequences spaced 32 bp apart (centre-to-centre) at the 186 pB binding site (4). However, DNase footprinting indicates that this binding causes strong distortion of the DNA between the two sites, suggesting that this is not the favoured spacing for CI. In contrast, no DNA distortion was apparent in the footprints on occupation of the three binding sites at pR, which are spaced two DNA turns apart (4).

Comparison of the CI–DNA wheel with the core nucleosome

A number of the features of the 186 CI–DNA complex are nucleosome-like but with significant differences. Both

complexes accommodate large stretches of DNA coiled around the outside of the protein. However, in CI wheels there is only a single, less bent DNA coil. DNA binds to nucleosomes with low sequence specificity, forming a large number of weak protein–DNA contacts, although there are sequence preferences dictated by the need for tight DNA bending (19). CI recognizes specific DNA sequences (4), yet CI wheels are also capable of substantial non-specific DNA binding, presumably because wrapping of DNA similarly provides multiple simultaneous weak contacts. We surmise that there is flexibility in the positioning of the HTH motifs around the outside of the wheel that allows these motifs to bind weakly to a variety of DNA sequences.

For both complexes, the length of DNA in contact with protein can vary, with some of the DNA unwrapped from the protein (20). This unwrapping seems to allow both protein complexes to accommodate DNA loops, in which the protein contacts non-contiguous DNA segments. For nucleosomes, this unwrapping and looping is believed to allow nucleosome repositioning along the DNA (21). Transfer of a CI wheel from one site to another could occur similarly; unwrapping the DNA at one site to allow simultaneous binding to a second site followed by competitive wrapping–unwrapping and release of the first site. The ability to accommodate DNA loops is proposed to allow nucleosomes to remain associated with DNA during the passage of RNA polymerase (22). During lysogeny, RNAP from pL must pass through CI wheels at pR to transcribe the CI gene. It is possible that this also can occur without the dissociation of CI from the DNA.

However, unlike nucleosomes, the symmetry of the CI wheel should allow it to move on the DNA without the need for DNA loops. By wrapping extra DNA at one end of the bound region and releasing it at the other, the wheel would simply 'roll' along the DNA. In contrast, the DNA entry and exit points in the nucleosome seem to be fixed, preventing such rolling.

A significant difference between the two complexes is that nucleosomes are able to interact with each other to form higher order structures, even in the absence of linker histones and other proteins (23), a key feature for their DNA packaging role. In contrast, we did not see any evidence for interactions between CI wheels, either on or off the DNA.

SUPPLEMENTARY DATA

Supplementary Data are available at NAR Online: Supplementary Tables 1–4, Supplementary Figures 1–8, Supplementary Methods and Supplementary References [24–27].

ACKNOWLEDGEMENTS

We thank Alexandra Ahlgren-Berg for plasmid constructions and Iain Murchland for assistance with Figure 2.

FUNDING

National Institutes of Health (NIH) [RGM084070A to L.F.]; Australian Research Council [DP110100824 to K.E.S., I.B.D. and L.F.]. Funding for open access charge: NIH (to L.F.) and other (to K.E.S.).

Conflict of interest statement. None declared.

REFERENCES

1. Dodd,I.B., Shearwin,K.E. and Sneppen,K. (2007) Modelling transcriptional interference and DNA looping in gene regulation. *J. Mol. Biol.*, **369**, 1200–1213.
2. Pinkett,H.W., Shearwin,K.E., Stayrook,S., Dodd,I.B., Burr,T., Hochschild,A., Egan,J.B. and Lewis,M. (2006) The structural basis of cooperative regulation at an alternate genetic switch. *Mol. Cell*, **21**, 605–615.
3. Dodd,I.B. and Egan,J.B. (2002) Action at a distance in CI repressor regulation of the bacteriophage 186 genetic switch. *Mol. Microbiol.*, **45**, 697–710.
4. Dodd,I.B. and Egan,J.B. (1996) DNA binding by the coliphage 186 repressor protein CI. *J. Biol. Chem.*, **271**, 11532–11540.
5. Shearwin,K.E., Dodd,I.B. and Egan,J.B. (2002) The helix-turn-helix motif of the coliphage 186 immunity repressor binds to two distinct recognition sequences. *J. Biol. Chem.*, **277**, 3186–3194.
6. Callen,B.P., Shearwin,K.E. and Egan,J.B. (2004) Transcriptional interference between convergent promoters caused by elongation over the promoter. *Mol. Cell*, **14**, 647–656.
7. Dodd,I.B., Kalionis,B. and Egan,J.B. (1990) Control of gene expression in the temperate coliphage 186. VIII. Control of lysis and lysogeny by a transcriptional switch involving face-to-face promoters. *J. Mol. Biol.*, **214**, 27–37.
8. Meijering,E., Jacob,M., Sarria,J.C., Steiner,P., Hirling,H. and Unser,M. (2004) Design and validation of a tool for neurite tracing and analysis in fluorescence microscopy images. *Cytometry A*, **58**, 167–176.
9. Schneider,C.A., Rasband,W.S. and Eliceiri,K.W. (2012) NIH Image to ImageJ: 25 years of image analysis. *Nat. Methods*, **9**, 671–675.
10. Dunlap,D., Zurla,C., Manzo,C. and Finzi,L. (2011) Probing DNA topology with Tethered particle motion. In: Peterman,E.J. and Wuite,G. (eds), *Methods in Molecular biology: Single-Molecule Analysis: Methods and Protocols*. Humana Press, NY, pp. 295–313.
11. Finzi,L. and Dunlap,D. (2003) Single-molecule studies of DNA architectural changes induced by regulatory proteins. *Methods Enzymol.*, **370**, 369–378.
12. Zurla,C., Manzo,C., Dunlap,D.D., Lewis,D.E.A., Adhya,S. and Finzi,L. (2009) Direct demonstration and quantification of long-range DNA looping by the lambda bacteriophage repressor. *Nucleic Acids Res.*, **37**, 2789–2795.
13. Finzi,L. and Dunlap,D.D. (2010) Single-molecule approaches to structure, kinetics and thermodynamics of transcriptional regulatory nucleoprotein complexes. *J. Biol. Chem.*, **285**, 18973–18978.
14. Manzo,C. and Finzi,L. (2010) Quantitative analysis of DNA looping kinetics from tethered particle motion experiments. In: Walter,N.G. (ed.), *Methods In Enzymology: Molecule Tools, Part B: Super-Resolution, Particle Tracking, Multiparameter, and Force Based Methods*. Elsevier Academic Press, Waltham, Massachussetts, pp. 199–220.
15. Nelson,P.C., Zurla,C., Brogioli,D., Beausang,J.F., Finzi,L. and Dunlap,D. (2006) Tethered particle motion as a diagnostic of DNA tether length. *J. Phys. Chem. B*, **110**, 17260–17267.
16. Wang,H., Finzi,L., Lewis,D. and Dunlap,D. (2009) AFM studies of the CI oligomers that secure DNA loops. *J. Pharm. Biotechnol.*, **10**, 494–501.
17. Fuentes-Perez,M.E., Gwynn,E.J., Dillingham,M.S. and Moreno-Herrero,F. (2012) Using DNA as a fiducial marker to study SMC complex interactions with the atomic force microscope. *Biophys. J.*, **102**, 839–848.

18. Shearwin,K.E. and Egan,J.B. (1996) Purification and self-association equilibria of the lysis-lysogeny switch proteins of coliphage 186. *J. Biol. Chem.*, **271**, 11525–11531.
19. Thåström,A., Lowary,P.T., Widlund,H.R., Cao,H., Kubista,M. and Widom,J. (1999) Sequence motifs and free energies of selected natural and non-natural nucleosome positioning DNA sequences. *J. Mol. Biol.*, **288**, 213–229.
20. Mellor,J. (2005) The dynamics of chromatin remodeling at promoters. *Mol. Cell*, **19**, 147–157.
21. Schiessel,H., Widom,J., Bruinsma,R.F. and Gelbart,W.M. (2001) Polymer reptation and nucleosome repositioning. *Phys. Rev. Lett.*, **86**, 4414–4417.
22. Studitsky,V.M., Clark,D.J. and Felsenfeld,G. (1995) Overcoming a nucleosomal barrier to transcription. *Cell*, **83**, 19–27.
23. Andrews,A.J. and Luger,K. (2011) Nucleosome structure(s) and stability: variations on a theme. *Annu. Rev. Biophys.*, **40**, 99–117.
24. Zurla,C., Franzini,A., Dunlap,D.D., Lewis,D.E.A., Adhya,S. and Finzi,L. (2006) Novel tethered particle motion analysis of CI protein-mediated DNA looping in the regulation of bacteriophage lambda. *Condens. Matter Phys.*, **18**, S225–S234.
25. Lewis,D., Le,P., Zurla,C., Finzi,L. and Adhya,S. (2011) Multilevel autoregulation of lambda repressor protein CI by DNA looping *in vitro*. *Proc. Natl Acad. Sci. USA*, **108**, 14807–14812.
26. Thundat,T., Zheng,X.Y., Sharp,S.L., Allison,D.P., Warmack,R.J., Joy,D.C. and Ferrell,T.L. (1992) Calibration of atomic force microscope tips using biomolecules. *Scanning Microscopy*, **4**, 903–910.
27. Miller,R., Vesenka,J. and Henderson,E. (1995) Tip reconstruction for the atomic force microscope. *SIAM J. Appl. Math.*, **55**, 1362–1371.